

Covariance-based sample selection for heterogenous data: Applications to gene expression and autism risk gene detection

Kevin Lin

Carnegie Mellon University, Statistics Department, Pittsburgh, PA

Han Liu

Northwestern University, Department of Electrical Engineering and Computer Science, Evanston, IL

Kathryn Roeder

Carnegie Mellon University, Statistics Department, Pittsburgh, PA*

March 23, 2022

Abstract

Risk for autism can be influenced by genetic mutations in hundreds of genes across the genome. Based on findings showing that genes with highly correlated gene expressions are functionally interrelated, “guilt by association” methods such as DAWN have been developed to identify autism risk genes. Previous research in this direction analyze the BrainSpan dataset, which contains gene expression of brain tissues from varying brain regions and developmental periods. Because the covariance among gene expression has been shown to vary with respect to the spatiotemporal properties of brain tissue, previous research was restricted to the subset of samples originating from a particular brain region and developmental period known to be associated with autism. While this was done to avoid the issue of heterogeneity, it also led to a potential loss of statistical power when detecting risk genes. In this article, we develop a new method to find a subset of samples that share the same population covariance matrix to retain a larger and more homogenous set of samples for the downstream DAWN analysis. Based on this analysis, we identify a risk gene set with greater enrichment in an independent study.

Keywords: Bootstrap covariance test, Microarray, Multiple testing with dependence

*This work was supported by NIMH grants R37MH057881 and R01MH109900.

1 Introduction

The genetic cause of autism spectrum disorder (ASD), a neurodevelopmental disorder that affects roughly 1-2% individuals in the United States, remains an open problem despite decades of research ([Autism and Investigators, 2014](#)). ASD is characterized primarily by impaired social functions and repetitive behavior ([Kanner et al., 1943](#); [Rutter, 1978](#)). To better understand this disorder, scientists identify specific genes that are liable for increasing the chance of developing ASD when damaged or mutated ([Sanders et al., 2015](#)). These genes are called risk genes. While breakthroughs in genomic technologies and the availability of large ASD cohorts have led to the discovery of dozens of risk genes, preliminary studies suggest there are hundreds of risk genes still unidentified ([Buxbaum et al., 2012](#)). In this work, we build upon the current statistical methodologies to further improve our ability to identify risk genes.

We focus on statistical methods that use gene co-expression networks to help identify risk genes. These networks are estimated from gene expression data from brain tissue. Since these gene co-expression networks provide insight into genes that regulate normal biological mechanisms in fetal and early brain development, it was hypothesized that risk genes that alter these mechanisms should be clustered in these networks ([Šestan et al., 2012](#)). Early findings confirmed this hypothesis ([Parikshak et al., 2013](#); [Willsey et al., 2013](#)). These results led to the development of the Detection Association With Networks (DAWN) algorithm, which uses a “guilt by association” strategy – identifying new risk genes based on their connectivity to previously identified risk genes ([Liu et al., 2014, 2015](#)). However, the previous DAWN analyses suffer from statistical limitations that we will investigate and resolve in this article.

We challenge previous analyses’ assumptions regarding the homogeneity of the covariance matrix in gene expression data. Previous DAWN analyses assume that gene expression samples from the same brain tissue type share the same covariance matrix. This assumption was influenced by the findings in [Kang et al. \(2011\)](#) and [Willsey et al. \(2013\)](#), which showed

that gene co-expression patterns differ among different brain regions and developmental periods on average. Statistically, this means that the covariance matrix among the gene expressions may differ with respect to the spatio-temporal properties of the brain tissue. Hence, previous DAWN analyses (Liu et al., 2014, 2015) use only samples from a particular brain tissue type chosen by the findings in Willsey et al. (2013) for their analyses. However, no further statistical analysis is performed to check for homogeneity of this specific subset of samples. In addition, since previous DAWN analyses limit themselves to a subset of gene expression samples, many other samples assumed to be heterogeneous are excluded. This leads to a potential loss of power when identifying risk genes.

To overcome these limitations, we aim to select a subset of gene expression samples in a data-driven way that is more homogenous and larger in sample size than the fixed subset used previously. We take advantage of the recent developments in high-dimensional covariance testing (Chang et al., 2015; Cai et al., 2013) to determine whether two gene expression datasets originating from different brain tissues share the same population covariance matrix. This is paired with a multiple-testing method called Stepdown that accounts for the dependencies among many hypothesis tests (Romano and Wolf, 2005; Chernozhukov et al., 2013). We show that tailoring the Stepdown method to perform many covariance tests leads to an improvement in identifying risk genes. This article addresses the numerous algorithmic challenges needed to implement this idea.

In Section 2, we describe the data and statistical model for heterogeneity in the covariance matrix. In Section 3, we provide a visual diagnostic to investigate the homogeneity assumptions of previous DAWN analyses. In Section 4, we describe the different stages of our procedure to find a subset of homogenous samples within a dataset. In Section 5, we illustrate the properties of our procedure on synthetic datasets. In Section 6, we apply our procedure on gene expression data to show that, when combined with DAWN, we identify an improved set of risk genes. Section 7 provides an overall summary and discussion.

2 Data and model background

Due to the challenge of obtaining and preserving brain tissue, datasets recording the gene expression patterns of brain tissue are rare. The BrainSpan project contributes one of the largest microarray expression datasets available (the “BrainSpan dataset” henceforth), sampling tissues from 57 postmortem brains with no signs of large-scale genomic abnormalities (Kang et al., 2011). Many studies have favored this dataset because its 1294 microarray samples capture the spatial and temporal changes in gene expression that occur in the brain during the entirety of development (De Rubeis et al., 2014; Cotney et al., 2015; Dong et al., 2014). While our paper focuses on this particular microarray expression dataset, our method would apply to other gene expression datasets such as RNA sequencing data.

The heterogeneity of gene expression due to the spatiotemporal differences in brain tissues presents statistical challenges. As documented in detail in Kang et al. (2011), the region and developmental period of the originating brain tissue contribute more to the heterogeneity than other variables such as sex and ethnicity. To understand this heterogeneity, we partition the dataset using the following schema. Each of the 1294 microarray samples is categorized into one of 16 *spatio-temporal windows*, or *windows* for short, depending on which brain region and developmental period the brain tissue is derived from. Within each window, all microarray samples originating from the same brain are further categorized into the same *partition*. There are 212 partitions in total. Figure 1 summarizes how many partitions and microarray samples belong in each window in the BrainSpan dataset. This schema allows us to model the microarray samples more realistically since the gene co-expression patterns vary greatly on average from window to window (Willsey et al., 2013). Additionally, Willsey et al. (2013) find that among all the windows, the known risk genes in Window 1B are most tightly co-expressed. Window 1B is highlighted in Figure 1 and contains the 107 microarray samples from the prefrontal cortex and primary motor-somatosensory cortex from 10 to 19 post-conceptual weeks. Due to this finding, previous DAWN analyses focus on all 107 samples from 10 partitions, assuming that these samples were homogenous without further

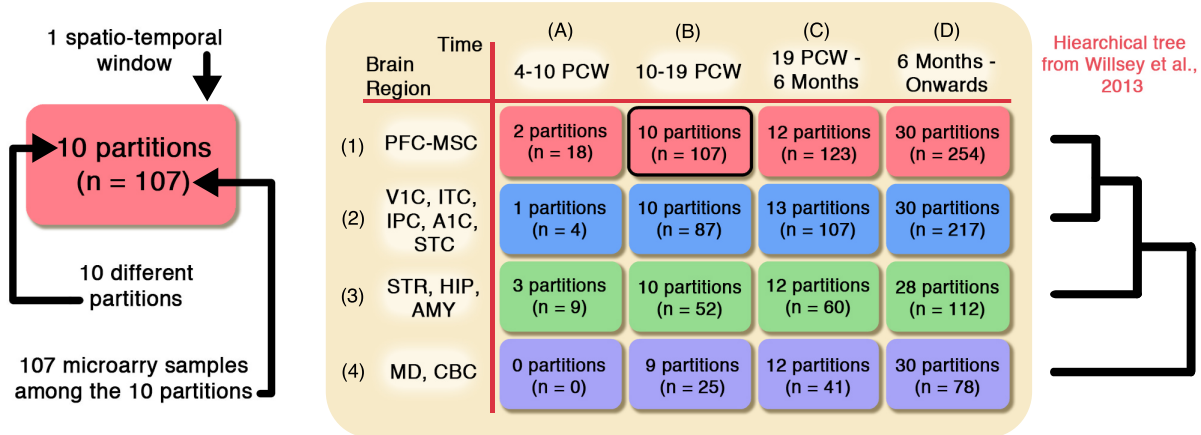


Figure 1: (Left) 107 microarray samples grouped by the originating 10 brains. This forms 10 different partitions. Since all these partitions originate from the same brain region and developmental period, they are further grouped into the same window. (Right) The 57 postmortem brains belong to 4 different developmental periods (columns). Here, PCW stands for post-conceptual weeks. Each brain is dissected and sampled at 4 different brain regions (rows), contributing 1 to 12 microarray samples per window (mean of 6). In total, over the 212 partitions, there are 1294 microarray samples, each measuring the expression of over 13,939 genes. Window 1B (outlined in black) is the window that previous work (Liu et al., 2015) focus on, and the hierarchical tree from Willsey et al. (2013) is shown to the right.

statistical investigation, and discard the remaining 1187 samples, (Liu et al., 2014, 2015). We seek to improve upon this heuristical sample selection procedure, first by formalizing a statistical model.

2.1 Statistical model

We use a Gaussian mixture model that assumes that microarray samples from the same partition are homogenous while samples from different partitions could be heterogeneous. For the p th partition, let $\mathbf{X}_1^{(p)}, \dots, \mathbf{X}_{n_p}^{(p)} \in \mathbb{R}^d$ denote n_p i.i.d. samples, and let $w(p)$ denote the window that partition p resides in. These n_p samples are drawn from either a Gaussian distribution with covariance Σ , or a Gaussian distribution with a different covariance matrix Σ_p . Our notation emphasizes that Σ is the covariance matrix shared among all partitions, while Σ_p may vary from partition to partition. A fixed but unknown parameter $\gamma_{w(p)} \in [0, 1]$

controls how frequently the partitions in window w are drawn from these two distributions, meaning it controls the amount of heterogeneity. For each partition p , this mixture model is succinctly described as,

$$I^{(p)} \sim \text{Bernoulli}(\gamma_{w(p)}),$$

$$\mathbf{X}_1^{(p)}, \dots, \mathbf{X}_{n_p}^{(p)} \stackrel{i.i.d.}{\sim} \begin{cases} N(\mathbf{0}, \Sigma) & \text{if } I^{(p)} = 1 \\ N(\mathbf{0}, \Sigma_p) & \text{otherwise,} \end{cases} \quad (2.1)$$

where $I^{(p)}$ is the latent variable that determines whether or not the samples in partition p have covariance Σ or Σ_p . With this model setup, our task becomes determining the set of partitions that originate from the covariance matrix Σ , which we will call

$$\mathcal{P} = \left\{ p : I^{(p)} = 1 \right\}. \quad (2.2)$$

The findings of [Kang et al. \(2011\)](#) and [Willsey et al. \(2013\)](#) inform us on how much heterogeneity to expect within a window via $\gamma_{w(p)}$. While analyses such as [Liu et al. \(2015\)](#) assume that all the samples in Window 1B are homogenous, it is noted in [Kang et al. \(2011\)](#) that sampling variability in brain dissection and in the proportion of white and gray matter in different brain tissues can cause variability in the gene co-expression patterns. This means that scientifically, we do not expect all the partitions in Window 1B to be homogenous (i.e., $\gamma_{w(p)} = 1$). Furthermore, [Willsey et al. \(2013\)](#) find a hierarchical clustering among the four brain regions. This is illustrated in [Figure 1](#), where the gene co-expression patterns in the brain regions represented in first row are most similar to those in the second row and least similar to those in the fourth row. The authors also find a smooth continuum of gene expression patterns across different developmental periods, represented as the columns of the table in [Figure 1](#). Hence, we expect $\gamma_{w(p)}$ to decrease smoothly as the window w becomes more dissimilar to Window 1B, in both the spatial and temporal direction.

2.2 Connections to other work

Other work use models similar to (2.1) on microarray expression data to tackle the different co-expression patterns among different tissues and subjects, but their methods differ from ours. One direction is to directly cluster the covariance matrices of each partition (Ieva et al., 2016). However, this approach does not account for the variability in the empirical covariance matrix, unlike our hypothesis-testing based method. Another approach is to explicitly model the population covariance matrix for each partition as the summation of a shared component and a partition-specific heterogenous component. This is commonly used in batch-correction procedures where the analysis removes the heterogeneous component from each partition (Leek and Storey, 2007). However, we feel such an additive model is too restrictive for analyzing the BrainSpan dataset, as we do not believe there is a shared covariance matrix across all windows of the brain. Instead, our approach will find specific set of partitions with statistically indistinguishable covariance matrices.

3 Elementary analysis

In this section, we develop a visual diagnostic to investigate if the 10 partitions in Window 1B used in previous work (Liu et al., 2014, 2015) are as homogeneous as these previous analyses assume. Using a hypothesis test for equal covariances, our diagnostic leverages the following idea: we divide the partitions into two groups and apply a hypothesis test to the samples between both groups. If all the partitions were truly drawn from distributions with equal covariances, then over many possible divisions, the empirical distribution of the resulting p-values should be roughly uniform. We can visualize this distribution by using a QQ-plot. The less uniform the p-values look, the less we are inclined to interpret our partitions to be all drawn from distributions with equal covariances. The following algorithm summarizes this diagnostic.

Algorithm 1: Covariance homogeneity diagnostic

1. Loop over trials $t = 1, 2, \dots, T$:

- (a) Randomly divide the selected partitions in the set $\widehat{\mathcal{P}}$ into two sets, $\widehat{\mathcal{P}}^{(1)}$ and $\widehat{\mathcal{P}}^{(2)}$, such that $\widehat{\mathcal{P}}^{(1)} \cup \widehat{\mathcal{P}}^{(2)} = \widehat{\mathcal{P}}$ and $\widehat{\mathcal{P}}^{(1)} \cap \widehat{\mathcal{P}}^{(2)} = \emptyset$.
- (b) For each partition $p \in \widehat{\mathcal{P}}^{(1)}$, center the samples $\mathbf{X}_1^{(p)}, \dots, \mathbf{X}_{n_p}^{(p)}$. Then aggregate all samples in $\widehat{\mathcal{P}}^{(1)}$ to form the set of samples

$$\mathcal{X} = \bigcup_{p \in \mathcal{P}^{(1)}} \{\mathbf{X}_1^{(p)}, \dots, \mathbf{X}_{n_p}^{(p)}\}.$$

Similarly, form the set of samples \mathcal{Y} from the set of partitions $\mathcal{P}^{(2)}$.

- (c) Compute the p-value for a hypothesis test that tests whether or not the samples in \mathcal{X} and \mathcal{Y} have the same covariance matrix.

2. Produce a QQ-plot of the resulting T p-values to see if empirical distribution of the p-values is close to a uniform distribution.

We remind the reader that the above procedure is a diagnostic. This is not necessarily a recipe for a goodness-of-fit test since the T p-values are not independent, which makes it difficult to analyze its theoretical properties. However, as we will demonstrate in later sections of this article, this diagnostic is nonetheless able to display large-scale patterns in our dataset.

3.1 Specification of covariance hypothesis test

To complete the above diagnostic's description, we describe the procedure to test for equality of covariance matrices. Let $\mathcal{X} = \{\mathbf{X}_1, \dots, \mathbf{X}_{n_1}\}$ and $\mathcal{Y} = \{\mathbf{Y}_1, \dots, \mathbf{Y}_{n_2}\}$ be n_1 and n_2 i.i.d. samples from d -dimensional distributions with covariance Σ_X and Σ_Y respectively, both with an empirical mean of $\mathbf{0}$. We define $\mathbb{X} \in \mathbb{R}^{n_1 \times d}$ and $\mathbb{Y} \in \mathbb{R}^{n_2 \times d}$ as the matrices

formed by concatenating these samples row-wise. Define the empirical covariance matrices as $\widehat{\Sigma}_X = \mathbb{X}^\top \mathbb{X}/n_1$, and $\widehat{\Sigma}_Y = \mathbb{Y}^\top \mathbb{Y}/n_2$, where we denote the individual elements of these matrices as $\widehat{\Sigma}_X = [\widehat{\sigma}_{X,ij}]_{1 \leq i,j \leq d}$ and likewise for $\widehat{\Sigma}_Y$. We now discuss two possible hypothesis tests for equal covariance, $H_0 : \Sigma_X = \Sigma_Y$, that we will consider in this article.

Method 1 (With normalization): The first method defines the test statistic according to [Chang et al. \(2015\)](#) which extends [Cai et al. \(2013\)](#). In these work, the authors note that if $\Sigma_X = \Sigma_Y$, then the maximum element-wise difference between Σ_X and Σ_Y is 0. Hence, [Chang et al. \(2015\)](#) defines the test statistic \widehat{T} as the maximum of squared element-wise differences between $\widehat{\Sigma}_X$ and $\widehat{\Sigma}_Y$, normalized by its variance. Specifically,

$$\widehat{T} = \max_{ij} (\widehat{t}_{ij}) \quad \text{where } \widehat{t}_{ij} = \frac{(\widehat{\sigma}_{X,ij} - \widehat{\sigma}_{Y,ij})^2}{\widehat{s}_{X,ij}/n_1 + \widehat{s}_{Y,ij}/n_2}, \quad i, j \in 1, \dots, d, \quad (3.1)$$

where $\widehat{s}_{X,ij} = \sum_{m=1}^{n_1} (\mathbb{X}_{mi} \mathbb{X}_{mj} - \widehat{\sigma}_{X,ij})^2/n_1$ is the empirical variance of the variance-estimator $\widehat{\sigma}_{X,ij}$, and $\widehat{s}_{Y,ij}$ is defined similarly.

Then, [Chang et al. \(2015\)](#) constructs an empirical null distribution of \widehat{T} under $H_0 : \Sigma_X = \Sigma_Y$ using the multiplier bootstrap ([Chernozhukov et al., 2013](#)). On each of the $b \in \{1, \dots, B\}$ trials, the multiplier bootstrap computes a bootstrapped test statistic $\widehat{T}^{(b)}$ by weighting each of the $n_1 + n_2$ observations by a standard Gaussian random variable drawn independently of all other variables, denoted collectively as $(g_1^{(b)}, \dots, g_{n_1}^{(b)}, g_{n_1+1}^{(b)}, \dots, g_{n_1+n_2}^{(b)})$. Specifically, we construct the bootstrap statistic for the b th trial as

$$\widehat{T}^{(b)} = \max_{ij} (\widehat{t}_{ij}^{(b)}) \quad \text{where } \widehat{t}_{ij}^{(b)} = \frac{(\widehat{\sigma}_{X,ij}^{(b)} - \widehat{\sigma}_{Y,ij}^{(b)})^2}{\widehat{s}_{X,ij}^{(b)}/n_1 + \widehat{s}_{Y,ij}^{(b)}/n_2}, \quad i, j \in 1, \dots, d, \quad (3.2)$$

where $\widehat{\sigma}_{X,ij}^{(b)} = \sum_{m=1}^{n_1} g_m^{(b)} (\mathbb{X}_{mi} \mathbb{X}_{mj} - \widehat{\sigma}_{X,ij})/n_1$ and $\widehat{\sigma}_{Y,ij}^{(b)} = \sum_{m=1}^{n_2} g_{n+m}^{(b)} (\mathbb{Y}_{mi} \mathbb{Y}_{mj} - \widehat{\sigma}_{Y,ij})/n_2$. We compute the p-value by counting the proportion of bootstrap statistics that are larger than the test statistic,

$$\text{p-value} = \frac{|\{b : |\widehat{T}^{(b)}| \geq |\widehat{T}|\}|}{B}.$$

[Chang et al. \(2015\)](#) prove that this test has asymptotically $1 - \alpha$ coverage under the null

hypothesis for distributions with sub-Gaussian and sub-exponential tails, even in the high-dimensional regime where $d \gg \max(n_1, n_2)$.

Method 2 (Without normalization): The second method is similar to the first, except we replace the denominators shown in (3.1) and (3.2) with 1, meaning we do not normalize the element-wise difference between the two covariance matrices Σ_X and Σ_Y by its variance. We also consider the absolute differences instead of the squared difference. Specifically, the test statistic is defined as

$$\hat{T} = \max_{ij} (\hat{t}_{ij}) \quad \text{where } \hat{t}_{ij} = |\hat{\sigma}_{X,ij} - \hat{\sigma}_{Y,ij}|, \quad i, j \in 1, \dots, d, \quad (3.3)$$

and we make a similar modification for its bootstrap counterpart, $\hat{T}^{(b)}$. While [Chang et al. \(2015\)](#) do not originally consider this formulation, as we will see in [Subsection 4.2](#), this alternative method offers practical computational advantages for our partition selection procedure. Using the techniques in [Chernozhukov et al. \(2013\)](#), it can be proven that this test statistic will still yield a hypothesis test with asymptotic $1 - \alpha$ coverage under the null. However, we will see later that the lack of normalizing the element-wise differences results in a less powerful test.

3.2 Application to BrainSpan

Equipped with a complete description of the diagnostic, we apply it to the BrainSpan dataset. Among the 10 partitions in Window 1B, we divide the partitions into two groups uniformly at random 500 times, and compute a p-value using Method 1 (with normalization) for each division using 200 bootstrap trials. The QQ-plot of the resulting p-values are shown in [Figure 2](#) (left), where we see that the p-values are biased towards 0. This implies the 10 partitions in Window 1B are heterogeneous since they do not seem to all share the same covariance matrix. Furthermore, we apply this diagnostic to all partitions in the BrainSpan dataset with 5 or more samples. This results in using only 125 of the 212 partitions shown in [Figure 1](#). The resulting p-values become more biased towards 0 ([Figure 2](#), right), implying

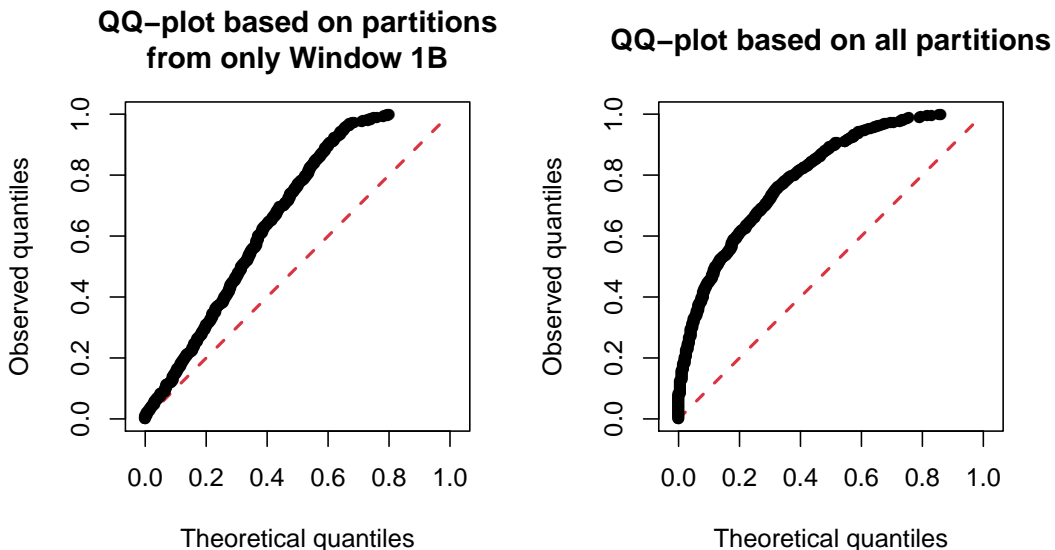


Figure 2: QQ-plots of the 500 p-values generated when applying our diagnostic to the BrainSpan dataset. (Left) The diagnostic using only the partitions in Window 1B, showing a moderate amount of heterogeneity. (Right) The diagnostic using all 125 partitions in the BrainSpan dataset, showing a larger amount of heterogeneity.

the dataset as a whole is more heterogeneous than the partitions in Window 1B. In the next section, we develop a method to resolve this issue by finding the largest subset of partitions possible among the 125 partitions in the BrainSpan dataset that share the same covariance matrix.

4 Methods

While we have discussed methods to test for equivalent covariance matrices between any two partitions in Section 3, we cannot directly apply these methods to the BrainSpan dataset without suffering a loss of power due to multiple testing. Since there are $r = 125$ partitions with more than 5 samples, applying the hypothesis test to each pair of partitions results in $\binom{r}{2} = 7750$ dependent p-values. These p-values are dependent since each of the r partitions is involved in $r - 1$ hypothesis tests. Hence, standard techniques such as a Bonferroni correction are too conservative when accounting for these dependencies, likely leading to a loss of power.

To properly account for this dependency, we introduce our Stepdown method in Subsection 4.1 that simultaneously tests all $\binom{r}{2}$ hypothesis tests. This bootstrap-based procedure is computationally expensive. However, depending on the test statistic used for the $\binom{r}{2}$ hypothesis tests, we offer a computationally faster alternative in Subsection 4.2. Afterward determining which of the $\binom{r}{2}$ pairs of partitions do not have statistically significant differences in their covariance matrices, we develop a clique-based method in Subsection 4.3 to select a specific set of partitions $\widehat{\mathcal{P}}$.

4.1 Stepdown method: multiple testing with dependence

We use a Stepdown method developed in Chernozhukov et al. (2013) to control the family-wise error rate. We tailor the bootstrap-based procedure to our specific setting in the algorithm below. We denote $\widehat{T}_{(i,j)}$ as the test statistic formed using either (3.1) or (3.3) to test if the covariance of samples between partition i and partition j are equal. Similarly, let $\widehat{T}_{(i,j)}^{(b)}$ denote the corresponding bootstrap statistics on the b th bootstrap trial. Here, $\text{quantile}(\{x_1, \dots, x_n\}; 1 - \alpha)$ represents the empirical $(1 - \alpha) \cdot 100\%$ quantile of the vector (x_1, \dots, x_n) .

Algorithm 2: Stepdown method

1. Initialize the list enumerating all $\binom{r}{2}$ null hypotheses corresponding to the set of partition pairs

$$\mathcal{L}(1) = \{(1, 2), \dots, (r - 1, r)\}.$$

2. Loop over steps $t = 1, 2, \dots$:

(a) Calculate \widehat{T}_ℓ for each $\ell \in \mathcal{L}(t)$, as stated in (3.1).

(b) For each bootstrap trial $b = 1, \dots, B$:

- i. Generate $N = \sum_p n_p$ i.i.d. Gaussian random variables, one for each sample in each partition, and compute $\widehat{T}_\ell^{(b)}$ for all $\ell \in \mathcal{L}(t)$, as stated in (3.2).

ii. Compute

$$\widehat{T}^{(b)} = \max \left\{ \widehat{T}_\ell^{(b)} : \ell \in \mathcal{L}(t) \right\}. \quad (4.1)$$

(c) Remove any $\ell \in \mathcal{L}(t)$ if

$$\widehat{T}_\ell \geq \text{quantile} \left(\{ \widehat{T}^{(1)}, \dots, \widehat{T}^{(b)} \}; 1 - \alpha \right).$$

If no elements are removed from $\mathcal{L}(t)$, return the null hypotheses corresponding to $\mathcal{L}(t)$. Otherwise, continue to step $t + 1$.

Using techniques in [Romano and Wolf \(2005\)](#) and [Chernozhukov et al. \(2013\)](#), it can be proven that this method has the following asymptotic family-wise error guarantee,

$$\mathbb{P} \left(\text{no true null hypothesis among } \mathcal{H} \text{ null hypotheses are rejected} \right) \geq 1 - \alpha + o(1). \quad (4.2)$$

The reason the Stepdown method is able to control the family-wise error without using a Bonferroni correction is because the $\binom{r}{2}$ bootstrapped statistics in each trial are derived from same N Gaussian random variables, hence preserves the dependencies among the $\binom{r}{2}$ tests. While we use the test statistics (3.1) and (3.3) when describing the Stepdown method, we note that this method applies to a broader family of test statistics. In the next subsection, we describe a computational acceleration of the Stepdown method as long as the test statistic satisfies additional requirements.

4.2 Computational extension for the Stepdown method

The largest drawback to the Stepdown method lies in its intensive computational cost. For r partitions, at least $\binom{r}{2}$ bootstrap statistics need to be computed in each bootstrap trial, each requiring a computational cost of $O(d^2 \cdot n_p)$. In this subsection, we reduce the computational cost by leveraging properties of the bootstrap statistics $\widehat{T}_{(i,j)}^{(b)}$.

Specifically, we consider only bootstrap statistics that satisfy the triangle inequality for

this computational extension. That is, for any bootstrap trial b and for any partitions i , j and k , we require that the bootstrap statistics satisfy

$$\widehat{T}_{(i,k)}^{(b)} \leq \widehat{T}_{(i,j)}^{(b)} + \widehat{T}_{(j,k)}^{(b)}. \quad (4.3)$$

This property can potentially save expensive calculations when calculating (4.1) in [Algorithm 2](#) by reducing the number of bootstrap statistics we need to explicitly calculate. Since we only care about the maximum bootstrap statistic $\widehat{T}^{(b)}$ in each trial, the triangle inequality gives an upper bound on the bootstrap statistic $\widehat{T}_{(i,k)}^{(b)}$ between partitions i and k , leveraging bootstrap statistics already calculated within a specific bootstrap trial. As we sequentially iterate through all pairs of partitions (i, k) , if the upper bound for $\widehat{T}_{(i,k)}^{(b)}$ is smaller than the current maximum bootstrap statistic within a specific bootstrap trial b , we do not need to explicitly compute $\widehat{T}_{(i,k)}^{(b)}$.

We mentioned the non-normalized variant of the hypothesis test (3.3) earlier in this article because its bootstrap statistic satisfies the triangle inequality (4.3). We describe a subroutine that leverages this property to compute $\widehat{T}^{(b)}$ in (4.1) by representing the individual bootstrap statistics $\widehat{T}_{(i,j)}^{(b)}$ as weighted edges in a graph. The algorithm uses Dijkstra’s algorithm to find the shortest path between vertices. This implicitly computes the upper bound in the bootstrap statistic between two partitions using the triangle inequality. This algorithm can provide substantial improvement in computational speed by leveraging the fact that determining the shortest path on a fully-dense graph has a computational complexity of $O(r^2)$, whereas computing $T_{(i,j)}^{(b)}$ has a computational complexity of $O(d^2 \cdot n_p)$.

Algorithm 3: Distance metric-based procedure to compute $\widehat{T}^{(b)}$

1. Form graph $G = (V, E)$ with r nodes and all $\binom{r}{2}$ edges, and initialize each edge to have a weight of infinity.
2. Arbitrarily construct a spanning tree \mathcal{T} and compute all $\widehat{T}_{(i,j)}^{(b)}$ ’s corresponding to edges $(i, j) \in \mathcal{T}$. Record $z = \max_{(i,j) \in \mathcal{T}} \widehat{T}_{(i,j)}^{(b)}$.

3. Construct a set of edges $\mathcal{S} = \mathcal{L}(t) \setminus \mathcal{T}$ which represents the bootstrap statistics between specific pairs of partitions that have yet to be computed.
4. While \mathcal{S} is not empty:
 - (a) Arbitrarily select an edge $(i, j) \in \mathcal{S}$ and remove it from \mathcal{S} . Compute the shortest-path distance from vertex i to j in G .
 - (b) If the shortest-path distance is larger than z , update the edge (i, j) to have weight $\widehat{T}_{(i,j)}^{(b)}$, and update z to be $\max(z, \widehat{T}_{(i,j)}^{(b)})$.
5. Return z .

Unfortunately, the hypothesis test using the normalized test statistic (3.1) does not satisfy the triangle inequality (4.3). Hence, while this variant of the hypothesis test is more powerful, it can not use the computational extension above.

4.3 Largest partial clique: selecting partitions based on testing results

After applying the covariance testing with the Stepdown method described in the previous two subsections, we have a subset of null hypotheses from \mathcal{H} that we accept. In this subsection, we develop a clique-based method to estimate \mathcal{P} , the subset of partitions that share the same covariance matrix defined in (2.2), from our accepted null hypotheses.

We conceptualize the task of selecting partitions as selecting vertices from a graph. Let $H_{0,(i,j)}$ denote the null hypothesis that the population covariance matrices for partition i and j are equal. Let $G = (V, E)$ be an undirected graph with vertices V and edge set E such that

$$V = \{1, \dots, r\}, \quad E = \{(i, j) : H_{0,(i,j)} \text{ is accepted by the Stepdown method}\}. \quad (4.4)$$

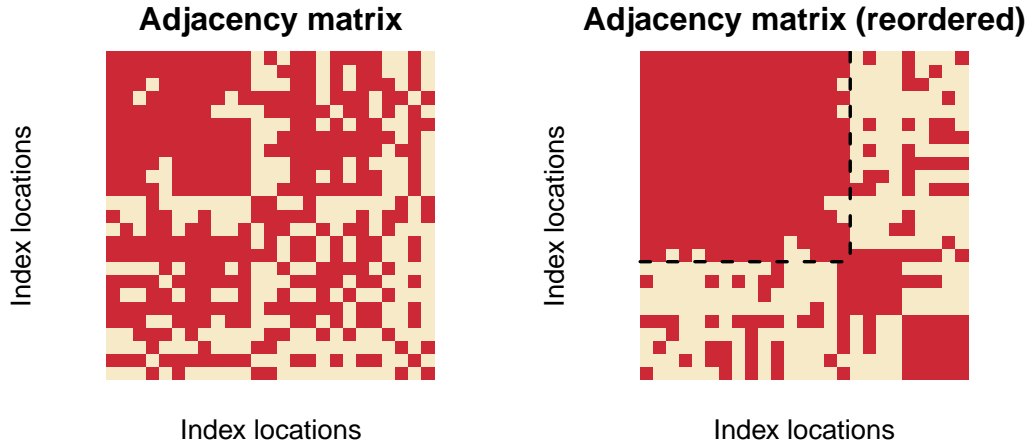


Figure 3: (Left) Visualization of an (example) adjacency matrix that can be formed using (4.4), where the i th row from top and column from the left denotes the i th vertex. A red square in position (i, j) denotes an edge between vertex i and j . (Right) Illustration of the desired goal. The rows and columns are reordered from the left figure, and the dotted box denotes the vertices that were found to be highly connected.

Since each of the $\binom{|\mathcal{P}|}{2}$ pairwise tests among the partitions in \mathcal{P} satisfies the null hypotheses, the vertices corresponding to \mathcal{P} would ideally form the largest clique in graph G . However, this ideal situation is unlikely to happen with finite samples, as illustrated by the theoretical guarantee in (4.2). Instead, there are likely to be a few missing edges in G among the vertices corresponding to \mathcal{P} . Hence, instead of selecting vertices that form the largest clique, we estimate \mathcal{P} by selecting the largest vertex set in G that is highly connected. This task is exemplified in Figure 3.

There are many algorithms such as spectral clustering that can find highly connected vertex sets, but many such algorithms lack a monotonicity property in practice. Specifically, suppose we have an algorithm \mathcal{A} that takes in a graph G and outputs a vertex set, denoted by $\mathcal{A}(G)$, and for two graphs G' and G , let $G' \subseteq G$ denote that every edge in G' is in G . Since we are trying to select a subset of highly connected vertices in G , it would natural to have the following property:

$$G' \subseteq G \quad \Rightarrow \quad |\mathcal{A}(G')| \leq |\mathcal{A}(G)|. \quad (4.5)$$

This is a desirable property since, intuitively, less partitions should be selected if our Stepdown method finds that more pairs of partitions to have significantly different covariance matrices. More importantly, this property is crucial in practice since the choice of α used by the Stepdown method in Subsection 4.1 is decided by the user. It can be shown that the parameter α and the graph G defined in (4.4) have the following relation,

$$\alpha' \leq \alpha \quad \Rightarrow \quad G' \subseteq G.$$

Hence, an algorithm that does not exhibit the property in (4.5) will be fragile – using a smaller α to accept more null hypotheses might counterintuitively result in less partitions being selected. As we will demonstrate in Section 5 through simulations, popular algorithms such as spectral clustering do not exhibit this property. Therefore, we develop a new algorithm that empirically exhibits the monotonicity property (4.5).

Our algorithm finds the largest partial clique in the graph formed by (4.4). We say a set of k vertices form an γ -partial clique if there are at least $\gamma \cdot \binom{k}{2}$ edges among these k vertices. A largest γ -partial clique is the largest vertex set that forms a γ -partial clique. We justify the choice to search for the largest γ -partial clique since, by construction of our model in (2.1), the prevalent covariance structure among the r partitions is the desired covariance structure we wish to estimate.

We describe the algorithm below. It starts by constructing a list containing all maximal cliques in the graph based on (4.4). A maximal clique is a vertex set that forms a clique but is not subset of a larger clique. The algorithm then proceeds by determining if the union of any two vertex sets forms a γ -partial clique. If so, this union of vertices is added to the list of vertex sets. The algorithm returns the largest vertex set in the list when all pairs of vertex sets are tried and no new γ -partial clique is found. We demonstrate in Section 5 that this algorithm exhibits the monotonicity property (4.5).

Algorithm 4: Clique-based selection

1. Form graph G based on (4.4).
2. Form \mathcal{Q} , the set of all vertex sets that form a maximal clique in G .
3. While there are vertex sets $A, B \in \mathcal{Q}$ the algorithm has not tried yet:
 - (a) Determine if $C = A \cup B$ forms a γ -partial clique in G . If so, add C as a new vertex set into \mathcal{Q} , with A and B as its two children sets.
4. Return the largest vertex set in \mathcal{Q} .

A naive implementation of the above algorithm would require checking if an exponential number of vertex set unions $C = A \cup B$ forms a γ -partial clique, and each check requires $O(r^2)$ operations. However, we are able to dramatically reduce the number of checks required by using the following heuristic: we only check whether the union of A and B forms a γ -partial clique if the union of two children sets, one from each A and B , forms a γ -partial clique. This heuristic allows us to exploit previous calculations and reduce computational costs. We implement this idea by using one hash table to record which vertex sets are children of other vertex sets, and another hash table to record if the union of two vertex sets forms a γ -partial clique. This idea is illustrated in Figure 4.

5 Simulation study

We perform empirical studies to show that our methods in Section 4 have more power and yield a better estimation of the desired covariance matrix Σ over conventional methods as the samples among different partitions are drawn from increasingly different distributions.

Setup: We generate synthetic data in different partitions, where the data in each partition has $n = 25$ samples and $d = 50$ dimensions, using the following schema. We construct

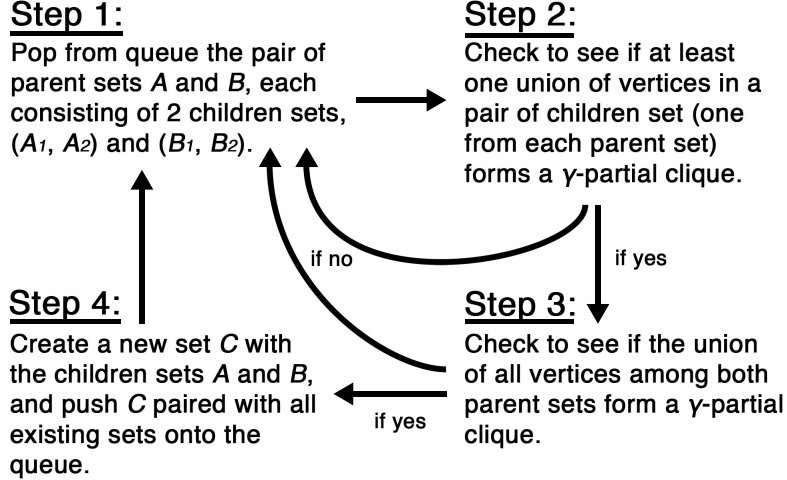


Figure 4: Schematic of [Algorithm 4](#). Step 2 is able to leverage hash tables which stores previous calculations to see if the union of vertices in a pair of children sets forms a γ -partial clique. This has a near-constant computational complexity. This can save tremendous computational time since Step 3, which checks if the union of vertices in both parent sets form a γ -partial clique, has a computational complexity of $O(r^2)$.

$\Sigma = [\Sigma_{i,j}]_{i,j=1}^d$ by $\Sigma_{i,j} = i \cdot (d - j + 1)/(d + 1)$. We generate the first $r_1 = 15$ partitions, where each partition consists of n i.i.d. samples drawn from $N(\mathbf{0}, \Sigma)$. For a fixed parameter $\beta \in (0, 1)$ which represents the flip percentage, we generate Σ' by uniformly randomly shuffling $(\beta \cdot 100)\%$ of the rows and their corresponding columns in Σ . We then generate the next $r_2 = 5$ partitions, where each partition consists of n i.i.d. samples drawn from $N(\mathbf{0}, \Sigma')$. Lastly, we generate the last $r_3 = 5$ partitions in the same fashion, by shuffling $(\beta \cdot 100)\%$ of the rows and their corresponding columns of Σ to generate Σ'' . Hence, we have a total of $r = r_1 + r_2 + r_3 = 25$ partitions where the desired goal is to discover that the first r_1 partitions share the same covariance structure. In this simulation study, β parameterizes how “easy” this task is, as a larger β means the hypothesis test described in [Section 3](#) has more power in distinguishing among samples drawn from the three covariance matrices Σ , Σ' and Σ'' . [Figure 5](#) visualizes the covariance matrices Σ and Σ' .

Multiple testing: We use the Stepdown method described in [Subsection 4.1](#) on our simulated data where $\beta = \{0, 0.1, 0.25, 0.75\}$ to see how the true positive rates and false

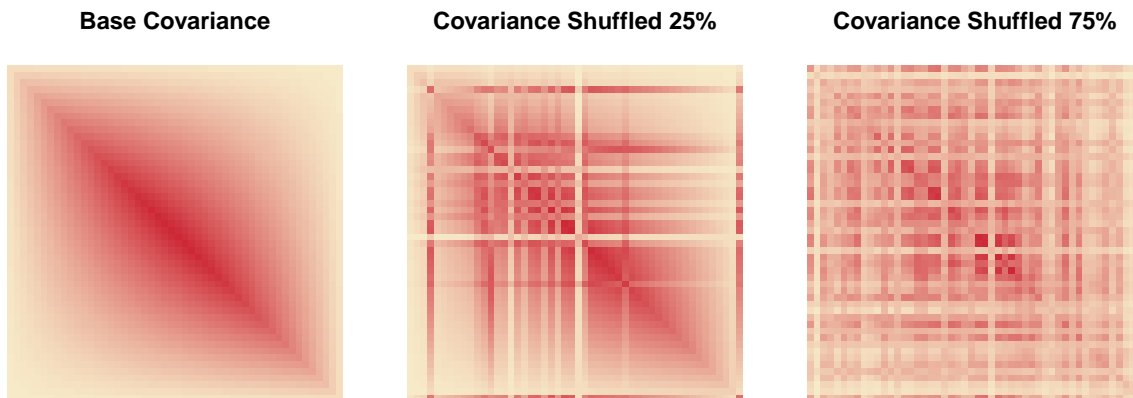


Figure 5: (Left) Visualization of the covariance matrix Σ where more saturated shades of red denotes larger values. (Middle) Visualization of one possible covariance matrix Σ' , generated by swapping $\beta = 0.25$ fraction of the rows and respective columns of Σ . (Right) Analogous to the middle plot, but swapping $\beta = 0.75$ fraction of the rows and respective columns of Σ . As the swap percentage increases, the difference between covariance matrices becomes more apparent.

positive rates vary with β . Let $\mathcal{L} = \{(i_1, j_1), (i_2, j_2), \dots\}$ denote the set of partition pairs that correspond to the accepted null hypothesis. Since our goal is to find the first r_1 partitions, we define the true positive rate to be

$$\text{true positive rate for hypotheses} = \frac{\left| \left\{ (i, j) \in \mathcal{L} : i \leq r_1 \text{ and } j \leq r_1 \right\} \right|}{\binom{r_1}{2}}.$$

Similarly, we define the false positive rate to be

$$\text{false positive rate for hypotheses} = \frac{\left| \left\{ (i, j) \in \mathcal{L} : i > r_1 \text{ or } j > r_1 \right\} \right|}{\binom{r}{2} - \binom{r_1}{2}}.$$

We plot the RoC curves visualizing the true and false positive rates in Figure 6. Each curve traces out the mean true and false positive rate over 20 simulations as α ranges from 0 (top-right of each plot) to 1 (bottom-left of each plot), where we use 1000 bootstrap trials per simulation. The left plot of Figure 6 represents the analysis that did not use the methods we develop in this article. There, we compute all $\binom{r}{2}$ p-values, one for each hypothesis test comparing two partitions, and accept hypotheses for varying levels of α after using a

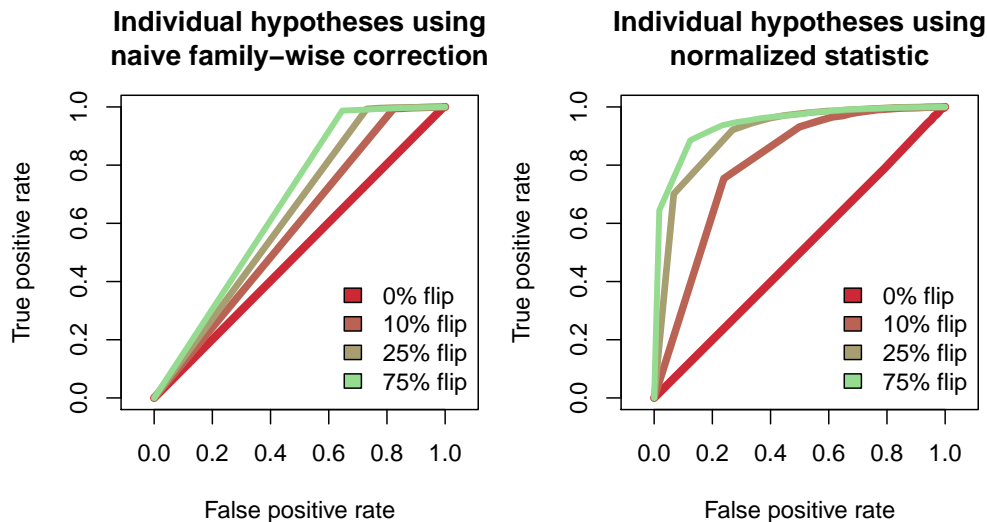


Figure 6: RoC curves for the accepted hypotheses, for settings where $\beta = (0, 0.1, 0.25, 0.75)$, where each curve traces out the results as α varies from 0 to 1. (Left) The curves resulting from using a Bonferroni correction to the $\binom{2}{2}$ individual hypothesis tests. (Right) The curves resulting from using the Stepdown method with the normalized statistic (3.1).

Bonferroni correction. The right plot shows the curves for the Stepdown method using the normalized statistic (3.1). In both plots, we see that as the flip percentage β increases, each method has more power. However, as we mentioned in Subsection 4.1, there is a considerable loss of power from the Stepdown method to the naive family-wise correction. This is because the Bonferroni correction is too conservative when accounting for dependencies. We show the RoC curves for the Stepdown method using the non-normalized statistic (3.3) in the appendix. It has less power than the Stepdown method using the normalized statistic (3.1), but more than the naive family-wise correction method.

Partition selection: Using the Stepdown method using the normalized statistic (3.1), we proceed to select the partitions as in Subsection 4.3 to understand the monotonicity property and see how the true and false positive rates for partitions vary with the flip percentage β .

The left figure of Figure 7 shows how certain methods to find highly connected vertices (4.4) fail the monotonicity property (4.5). Here, we compare our largest partial clique

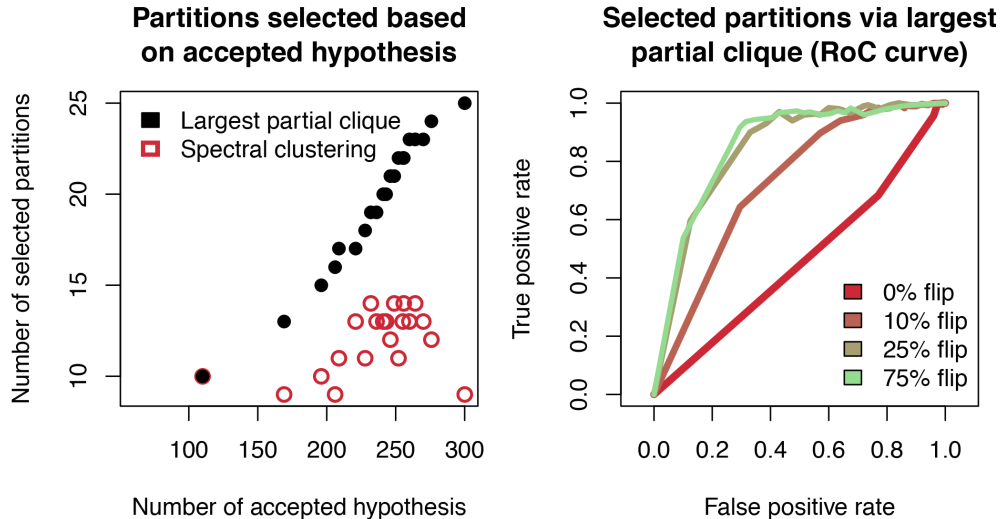


Figure 7: (Left) Number of selected partitions for a particular simulated dataset as the number of accepted hypotheses varies with the family-wise error rate α . (Right) Similar RoC curves to Figure 6, but for selected partitions after using the Stepdown method with the normalized test statistic.

method, described in Subsection 4.3, against spectral clustering, a method used in network analyses designed to find highly connected vertices in degree-corrected stochastic block models (Lei and Zhu, 2017). Both methods are applied to the same simulated dataset and receive the same set of accepted hypotheses as the family-wise error rate α varies. Recall that since the Stepdown method accepts more hypotheses as α increases, the graph formed by (4.4) becomes denser as α increases. However, as we see in Figure 7 (left), the number of partitions selected by spectral clustering sometimes decreases as number of accepted hypotheses increases, hence violating the desired monotonicity property. On the other hand, we see that our largest partial clique method empirically satisfies the monotonicity property. Here, we set our algorithm to find the largest 0.95-partial clique, and it empirically satisfies the monotonicity property in the simulation suite.

The right figure of Figure 7 shows the RoC curves for varying β as the family-wise error rate α varies. This figure is closely related to the right plot of Figure 6. We use our largest partial clique method to find the largest 0.95-partial clique. Let $\hat{\mathcal{P}}$ denote the selected set of

partitions. Similar to before, we define the true and false positive rate in this setting as

$$\begin{aligned} \text{true positive rate for partitions} &= \frac{\left| \left\{ p \in \widehat{\mathcal{P}} : p \leq r_1 \right\} \right|}{r_1}, \\ \text{false positive rate for partitions} &= \frac{\left| \left\{ p \in \widehat{\mathcal{P}} : p > r_1 \right\} \right|}{r_2 + r_3}. \end{aligned}$$

We see that the power of the largest partial clique method increases as β increases, as expected.

Covariance estimation: Finally, we show that our method is able to improve the downstream covariance estimation compared to other approaches. To do this, we use four different methods to select partitions and compute the empirical covariance matrix among the samples in those partitions. The first three methods resemble analyses that could be performed on the BrainSpan dataset in practice. The first method uses the procedure we develop. The second method always selects all the partitions, which resembles using all the partitions in the BrainSpan dataset. The third method always selects the same 5 partitions – 3 partitions contain samples drawn from $N(\mathbf{0}, \Sigma)$, while the other 2 partitions contain samples from each of the remaining two distributions. This resembles previous work (Liu et al., 2015) that consider only partitions in Window 1B. For comparison, the last method resembles an oracle that selects exactly the k_1 partitions containing samples drawn from $N(\mathbf{0}, \Sigma)$.

Figure 8 shows that our partition selection procedure performs almost as well as the oracle method over varying flip percentages β . This figure shows the mean spectral error of the estimated covariance matrix for each method and flip percentage over 10 trials. Notice that for low β , our method and the method using all partitions yield a smaller spectral error than the oracle method. This is because for low β , the covariance matrices Σ , Σ' , and Σ'' are almost indistinguishable. However, as β increases, the differences among Σ , Σ' , and Σ'' grows. This means methods that do not adaptively choose which partitions to select become increasingly worse. However, our procedure remains competitive, performing almost as if it

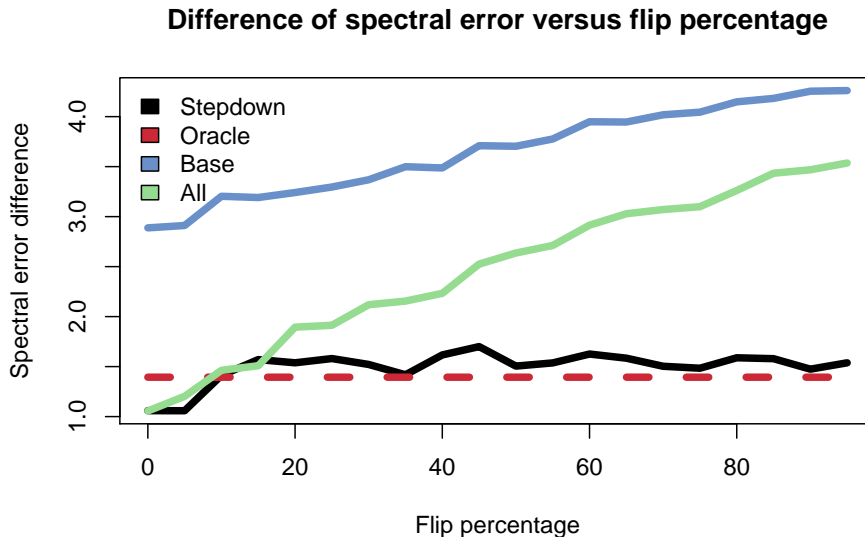


Figure 8: The mean spectral error of each method’s downstream estimated covariance matrix for varying flip percentage β . The four methods to select partitions shown are our method for $\alpha = 0.7$ (red), the method that selects all partitions (green), the method that selects a fixed set of 5 partitions (blue), and the method that selects exactly the partitions that contain samples drawn from $N(0, \Sigma)$ (black).

knew which partitions contain samples drawn from $N(0, \Sigma)$.

6 Application on BrainSpan study

6.1 Partition selection

We analyze the BrainSpan dataset using our entire selection procedure to find partitions matching the scientific intuition described in Willsey et al. (2013) and yielding better diagnostic results compared to those in Section 3. To perform this analysis, we select partitions based on only the 200 genes with the largest risk score according to an external dataset (De Rubeis et al., 2014). We use the Stepdown method with the normalized statistic (3.1) for 200 bootstrap trials and family-wise error level $\alpha = 0.1$. This simultaneously finds which null hypotheses are accepted among the $\binom{125}{2}$ hypotheses tested. Based on these results,

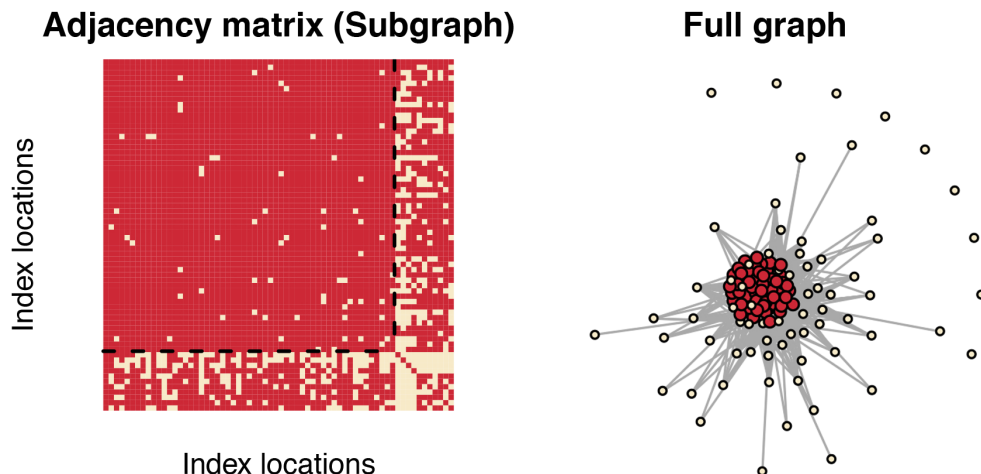


Figure 9: (Left) The adjacency matrix of a subgraph of G , where each row and corresponding column represents a different node, similar to Figure 3. A red pixel corresponds to an edge between two nodes, while a pale pixel represents no edge. The subgraph correspond to all the 55 selected partitions and 10 randomly chosen partitions not selected. (Right) The graph G containing all 125 nodes. Red nodes correspond to selected partitions, while pale nodes correspond to partitions not selected.

we use our clique-based selection method to select the partitions that form the maximal 0.95-partial clique. To break ties between maximal partial cliques, we use the clique with the most partitions in Window 1B.

We visualize the results of the Stepdown method in Figure 9, illustrating that our method finds 55 partitions which do not have significantly different covariance matrices. Because each null hypothesis corresponds to a pair of partitions, we form the graph G connecting pairs of partitions corresponding to the accepted null hypotheses, as described in (4.4). The left figure in Figure 9 shows a subgraph of G as an adjacency matrix, while the right figure shows the graph with all 125 nodes. The nodes in this graph are laid out using a standard layout algorithm so highly connected sets of nodes are placed compactly (Fruchterman and Reingold, 1991). Hence, we can see that the 55 partitions we select correspond to 55 nodes in G that are highly connected. These 55 partitions collectively contain 596 microarray samples.

We visualize the proportion of selected partitions per window in the BrainSpan dataset in

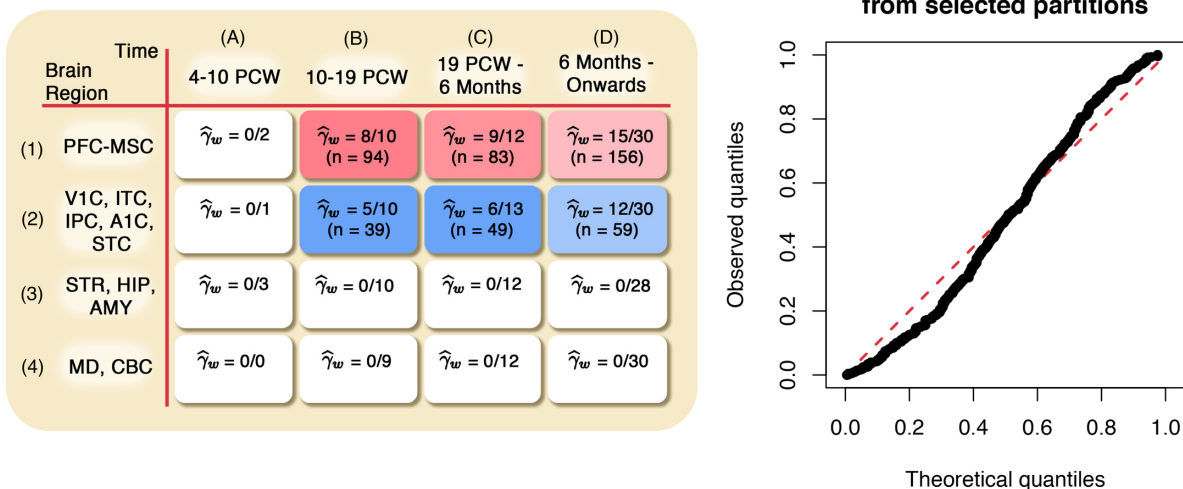


Figure 10: (Left) The number of partitions and samples (n) selected within each window. Partitions from 6 different windows are chosen, and the estimated γ_w is empirical fraction of selected partitions within each window. The more vibrant colors display a higher value of $\hat{\gamma}_w$. (Right) A QQ-plot of the 500 p-values generated when applying our diagnostic to the 55 selected partitions, similar in style to Figure 2. Compared to Figure 2, these selected partitions are more homogenous.

Figure 10 (left) to demonstrate that our findings are consistent with the findings in Willsey et al. (2013). As mentioned in Section 2, Willsey et al. (2013) find that partitions in Window 1B are mostly homogenous and are enriched for tightly clustered risk genes. The authors also found that, on average, gene expression varies smoothly across developmental periods, meaning there is greater correlation between the expressions of adjacent developmental windows. The authors also estimate a hierarchical clustering among the four brain regions. Indeed, our results match these finding. We select a large proportion of partitions in Window 1B, and the proportion of selected partitions decreases as the window represents older developmental periods as well as brain regions more dissimilar to Window 1B.

Lastly, we apply the same diagnostic as in Section 3 to show in Figure 10 (right) that the 596 samples within our 55 selected partitions are much more homogenous than the 107 samples among the 10 partitions in Window 1B. The p-values we obtain after 500 divisions are much closer to uniform than those shown in Section 3. To re-emphasize, we interpret this result as a diagnostic, not as a formal goodness-of-fit test as our p-values are not independent,

and the partitions were selected based on the BrainSpan data.

6.2 Gene network and detected risk genes

DAWN uses two datasets of genetic information to identify risk genes. The first dataset has been the primary focus of this article so far. It contains the microarray samples that our method selected from the BrainSpan dataset. The second dataset contains risk scores for each gene based on genetic variation found in individuals with ASD (He et al., 2013; De Rubeis et al., 2014). As mentioned in Section 1, DAWN combines these two datasets and uses a “guilt-by-association” strategy to identify risk genes. Specifically, it first estimates a gene co-expression network using the microarray samples, and then identifies risk genes that either have a high risk score or are connected to many other genes with high risk scores.

Figure 11 illustrates the flowchart of how DAWN combines the gene co-expression network with the risk scores. The first step uses the method we developed in Section 4 to select 55 partitions from the BrainSpan dataset, as stated in Subsection 6.1. In the second step, DAWN estimates a Gaussian graphical model from the 596 samples in these partitions to represent the gene co-expression network. We use neighborhood selection to estimate this Gaussian graphical model (Meinshausen and Bühlmann, 2006). In the last step, DAWN identifies risk genes using a Hidden Markov random field model to combine the Gaussian graphical model with the risk scores. The details are in Liu et al. (2015), but in short, this procedure assumes a mixture model of the risk scores between risk genes and non-risk genes, and the probability that a gene is a risk gene depends on the graph structure. To enable a fair comparison between our results and those in Liu et al. (2015), we apply the authors’ gene screening method to analyze only the most important 6670 genes, set all the tuning parameters to be the same, and identify the same number of risk genes.

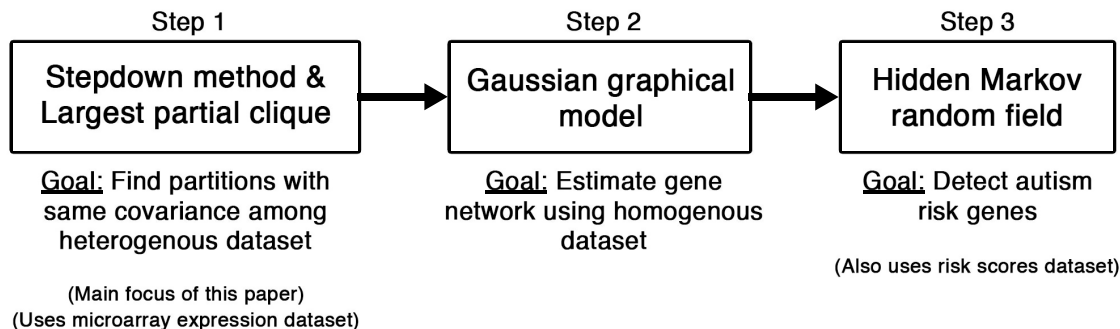


Figure 11: Flowchart of how our partition selection procedure (Stepdow method and largest partial clique) is used downstream to find risk genes.

6.3 Investigation on detected risk genes

We demonstrate that the 246 risk genes we identify are more promising than those identified in Liu et al. (2015) since we obtain a greater enrichment of genes identified in an independent study. Specifically, Iossifov et al. (2014) found 251 genes with new instances of de novo loss-of-function (dnLoF) mutations not already factored into the risk scores used in our DAWN analysis. DnLoF mutations are mutations present in an autistic child but not in either parents that cause genes to lose their functionality. These 251 genes with dnLoF mutations are natural candidates to compare our risk genes against since many separate studies found twice as many dnLoF mutations in individuals with ASD than individuals without (Neale et al., 2012; Iossifov et al., 2012; Sanders et al., 2012; O’Roak et al., 2012). This means dnLoF mutations contain the most signal among all forms of genetic variation. Hence, we are hoping for as many of our 246 risk genes to overlap with these 251 genes with new dnLoF mutations. However, since dnLoF mutations are rare events, we realistically do not expect a high overlap percentage. For example, De Rubeis et al. (2014) sequenced more than two thousand ASD trios but found less than two dozen genes with more than one dnLoF mutations.

We find that 22 of our 246 risk genes (8.9%) had additional dnLoF mutations in Iossifov et al. (2014), which is an improvement over the previous finding in Liu et al. (2015) where only 17 of 246 risk genes (6.9%) overlapped. These 22 genes are ADNP, ANK2, ARID1B,

CHD8, DIP2A, DSCAM, DYRK1A, FOXP1, ILF2, INTS6, KDM5B, KDM6B, MED13L, NCKAP1, NINL, OR52M1, PHF2, POGZ, RANBP17, RIMS1, SPAST, and WDFY3. This improvement of 5 genes represents a 129% increase improvement in the number of overlapped genes.

Furthermore, these 22 overlapped risk genes are robust to the family-wise error control α used in our Stepdown method in Section 4. We apply our procedure to a range of α values between 0.05 and 0.35 at intervals of 0.025. This results in 13 different sets of risk genes, one for each value of α . In 8 or more of these risk gene sets, we find the same 21 of 22 overlapped risk genes (95%). In fact, the 246 risk genes themselves are also empirically robust to α . Among the 13 risk gene sets, 209 of 246 risk genes (85%) were identified 8 or more times. All together, our results show that our method is able to identify risk genes that are more promising than before, and this finding is robust with respect to the tuning parameter α .

7 Conclusion and discussions

In this article, we develop a procedure to select partitions with statistically indistinguishable covariance matrices in order to identify risk genes. Our procedure first applies a Stepdown method to simultaneously test all $\binom{r}{2}$ hypotheses, one for testing whether or not each pair of partitions share the same population covariance matrix. The Stepdown method is critical since it can account for the dependencies among all $\binom{r}{2}$ hypotheses via bootstrapping the joint null distribution. Then, our procedure uses a clique-based selection method to select the partitions based on the accepted null hypotheses. The novelty in this latter method is its ability to preserve monotonicity, a property stating that less partitions should be selected as the number of accepted null hypotheses is smaller. We demonstrate empirically that the our method achieves this property while common methods such as spectral clustering do not. When we apply our entire procedure to the BrainSpan dataset as part of the DAWN analysis, we find scientifically meaningful partitions based on the results in [Willsey et al. \(2013\)](#). We also find that a higher percentage of our risk genes overlap with the genes identified in an

independent study (Iossifov et al., 2014) compared to previous work (Liu et al., 2015). This result is robust with respect to the tuning parameter of our procedure.

The theoretical role of the family-wise error level α is not well understood mathematically. Specifically, while (4.2) provides a theoretical guarantee about the set of null hypothesis accepted, we would like to prove a theoretical guarantee about the set of selected partitions $\widehat{\mathcal{P}}$. During the development of this article, it became clear that guarantees on $\widehat{\mathcal{P}}$ cannot be provided unless we understand the power of the Stepdown method. This will be investigated in future work.

Our procedure is applied directly to help identify risk genes for ASD, but this line of work has broader implications in genetics. Due to the improvement of high throughput technologies, it has become increasingly accessible to gather large amounts of gene expression data. This includes both microarray and RNA sequencing data. However, as we have seen in this article, gene expression patterns can vary wildly among different tissues. Hence, it is challenging to select samples that are relevant for specific scientific tasks. Beyond analyzing brain tissues, Greene et al. (2015) develop procedures to select relevant samples amongst a corpus of microarray expression data to estimate gene co-expression networks for different tissue types. While Greene et al. (2015) currently contains no statistical foundation, our work provides a possible statistical direction for this research field to move towards.

Acknowledgments: We thank Bernie Devlin and Lambertus Klei for the insightful discussions about our analysis and results. We thank Li Liu and Ercument Cicek for providing the code used in Liu et al. (2015) to build off of.

References

- Autism and Investigators, D. D. M. N. S. Y. . P. (2014). Prevalence of autism spectrum disorder among children aged 8 years - Autism and developmental disabilities monitoring network, 11 sites, United States, 2010. *Morbidity and Mortality Weekly Report: Surveillance Summaries*, 63(2):1–21.
- Buxbaum, J. D., Daly, M. J., Devlin, B., Lehner, T., Roeder, K., State, M. W., and The Autism Sequencing

- Consortium (2012). The Autism Sequencing Consortium: Large-scale, high-throughput sequencing in autism spectrum disorders. *Neuron*, 76(6):1052–1056.
- Cai, T., Liu, W., and Xia, Y. (2013). Two-sample covariance matrix testing and support recovery in high-dimensional and sparse settings. *Journal of the American Statistical Association*, 108(501):265–277.
- Chang, J., Zhou, W., Zhou, W.-X., and Wang, L. (2015). Comparing large covariance matrices under weak conditions on the dependence structure and its application to gene clustering. *arXiv preprint arXiv:1505.04493*.
- Chernozhukov, V., Chetverikov, D., Kato, K., et al. (2013). Gaussian approximations and multiplier bootstrap for maxima of sums of high-dimensional random vectors. *The Annals of Statistics*, 41(6):2786–2819.
- Cotney, J., Muhle, R. A., Sanders, S. J., Liu, L., Willsey, A. J., Niu, W., Liu, W., Klei, L., Lei, J., and Yin, J. (2015). The autism-associated chromatin modifier CHD8 regulates other autism risk genes during human neurodevelopment. *Nature communications*, 6.
- De Rubeis, S., He, X., Goldberg, A. P., Poultney, C. S., Samocha, K., Cicek, A. E., Kou, Y., Liu, L., Fromer, M., Walker, S., et al. (2014). Synaptic, transcriptional and chromatin genes disrupted in autism. *Nature*, 515(7526):209–215.
- Dong, S., Walker, M. F., Carriero, N. J., DiCola, M., Willsey, A. J., Adam, Y. Y., Waqar, Z., Gonzalez, L. E., Overton, J. D., Frahm, S., et al. (2014). De novo insertions and deletions of predominantly paternal origin are associated with autism spectrum disorder. *Cell reports*, 9(1):16–23.
- Fruchterman, T. M. and Reingold, E. M. (1991). Graph drawing by force-directed placement. *Software: Practice and experience*, 21(11):1129–1164.
- Greene, C. S., Krishnan, A., Wong, A. K., Ricciotti, E., Zelaya, R. A., Himmelstein, D. S., Zhang, R., Hartmann, B. M., Zaslavsky, E., and Sealfon, S. C. (2015). Understanding multicellular function and disease with human tissue-specific networks. *Nature genetics*.
- He, X., Sanders, S. J., Liu, L., De Rubeis, S., Lim, E. T., Sutcliffe, J. S., Schellenberg, G. D., Gibbs, R. A., Daly, M. J., Buxbaum, J. D., et al. (2013). Integrated model of *de novo* and inherited genetic variants yields greater power to identify risk genes. *PLoS Genetics*, 9(8):e1003671.
- Ieva, F., Paganoni, A. M., and Tarabelloni, N. (2016). Covariance-based clustering in multivariate and functional data analysis. *The Journal of Machine Learning Research*, 17(1):4985–5005.

- Iossifov, I., O’Roak, B. J., Sanders, S. J., Ronemus, M., Krumm, N., Levy, D., Stessman, H. A., Witherspoon, K. T., Vives, L., Patterson, K. E., et al. (2014). The contribution of de novo coding mutations to autism spectrum disorder. *Nature*, 515(7526):216–221.
- Iossifov, I., Ronemus, M., Levy, D., Wang, Z., Hakker, I., Rosenbaum, J., Yamrom, B., Lee, Y.-h., Narzisi, G., Leotta, A., et al. (2012). *De novo* gene disruptions in children on the autistic spectrum. *Neuron*, 74(2):285–299.
- Kang, H. J., Kawasawa, Y. I., Cheng, F., Zhu, Y., Xu, X., Li, M., Sousa, A. M., Pletikos, M., Meyer, K. A., Sedmak, G., et al. (2011). Spatio-temporal transcriptome of the human brain. *Nature*, 478(7370):483–489.
- Kanner, L. et al. (1943). Autistic disturbances of affective contact. *Nervous child*, 2(3):217–250.
- Leek, J. T. and Storey, J. D. (2007). Capturing heterogeneity in gene expression studies by surrogate variable analysis. *PLoS Genet*, 3(9):e161.
- Lei, J. and Zhu, L. (2017). Generic sample splitting for refined community recovery in degree corrected stochastic block models. *Statistica Sinica*, 27:1639–1659.
- Liu, L., Lei, J., and Roeder, K. (2015). Network assisted analysis to reveal the genetic basis of autism. *The Annals of Applied Statistics*, 9(3):1571–1600.
- Liu, L., Lei, J., Sanders, S. J., Willsey, A. J., Kou, Y., Cicek, A. E., Klei, L., Lu, C., He, X., and Li, M. (2014). DAWN: a framework to identify autism genes and subnetworks using gene expression and genetics. *Mol Autism*, 5:22.
- Meinshausen, N. and Bühlmann, P. (2006). High-dimensional graphs and variable selection with the Lasso. *The Annals of Statistics*, pages 1436–1462.
- Neale, B. M., Kou, Y., Liu, L., Ma’ayan, A., Samocha, K. E., Sabo, A., Lin, C.-F., Stevens, C., Wang, L.-S., Makarov, V., et al. (2012). Patterns and rates of exonic *de novo* mutations in autism spectrum disorders. *Nature*, 485(7397):242–245.
- O’Roak, B. J., Vives, L., Girirajan, S., Karakoc, E., Krumm, N., Coe, B. P., Levy, R., Ko, A., Lee, C., Smith, J. D., et al. (2012). Sporadic autism exomes reveal a highly interconnected protein network of *de novo* mutations. *Nature*, 485(7397):246–250.
- Parikshak, N. N., Luo, R., Zhang, A., Won, H., Lowe, J. K., Chandran, V., Horvath, S., and Geschwind, D. H. (2013). Integrative functional genomic analyses implicate specific molecular pathways and circuits in autism. *Cell*, 155(5):1008–1021.

- Romano, J. P. and Wolf, M. (2005). Exact and approximate stepdown methods for multiple hypothesis testing. *Journal of the American Statistical Association*, 100(469):94–108.
- Rutter, M. (1978). Diagnosis and definition of childhood autism. *Journal of autism and childhood schizophrenia*, 8(2):139–161.
- Sanders, S. J., He, X., Willsey, A. J., Ercan-Sencicek, A. G., Samocha, K. E., Cicek, A. E., Murtha, M. T., Bal, V. H., Bishop, S. L., Dong, S., et al. (2015). Insights into autism spectrum disorder genomic architecture and biology from 71 risk loci. *Neuron*, 87(6):1215–1233.
- Sanders, S. J., Murtha, M. T., Gupta, A. R., Murdoch, J. D., Raubeson, M. J., Willsey, A. J., Ercan-Sencicek, A. G., DiLullo, N. M., Parikshak, N. N., Stein, J. L., et al. (2012). *De novo* mutations revealed by whole-exome sequencing are strongly associated with autism. *Nature*, 485(7397):237–241.
- Šestan, N. et al. (2012). The emerging biology of autism spectrum disorders. *Science*, 337(6100):1301–1303.
- Willsey, A. J., Sanders, S. J., Li, M., Dong, S., Tebbenkamp, A. T., Muhle, R. A., Reilly, S. K., Lin, L., Fertuzinhos, S., Miller, J. A., et al. (2013). Coexpression networks implicate human midfetal deep cortical projection neurons in the pathogenesis of autism. *Cell*, 155(5):997–1007.

A Code and dataset

The R code for replicating all analyses and figures in this article are hosted on GitHub in the repository https://github.com/linnylin92/covariance_selection. The two major datasets used in this article are also included in the repository. The first dataset is the BrainSpan microarray samples collected by (Kang et al., 2011). While the original dataset is publicly available on GEO (<https://www.ncbi.nlm.nih.gov/geo/query/acc.cgi?acc=GSE25219>), we provide a locally preprocessed dataset, which was created to be amendable for our analysis in R. The second dataset is the p-value risk scores for the genes obtained applying the TADA framework (He et al., 2013) to the data available in (De Rubeis et al., 2014).

B Brain region details

There are four primary brain regions, each containing smaller, subregions.

- **PFC-MS**C: The prefrontal cortex (PFC) and primary motor-somatosensory cortex (MSC) consists of six smaller regions: primary motor cortex, primary somatosensory cortex, ventral prefrontal cortex, medial prefrontal cortex, dorsal prefrontal cortex and orbital prefrontal cortex.
- **V1C, ITC, IPC, A1C, STC**: A region consisting of the primary visual cortex (V1C), inferior temporal cortex (ITC), primary auditory cortex (A1C), and superior temporal cortex (STC).
- **STR, HIP, AMY**: A region consisting of the stratum (STR), hippocampal anlage or hippocampus (HIP) and amygdala (AMY).
- **MD, CBC**: A region consisting of the mediodorsal nucleus of the thalamus (MD) and the cerebellar cortex (CD).

C Non-normalized analysis

We show the RoC curve for the Stepdown method using the non-normalized test statistic (3.3) in Figure 12 and demonstrate that it is less powerful than its normalized counterpart. The simulation setup shown in is exactly the same as the one described in Section 5. While we do not use the non-normalized test statistic in the BrainSpan analysis afterwards, we believe that test statistics that enable the computation acceleration (Subsection 4.2) can be further investigated in future work.

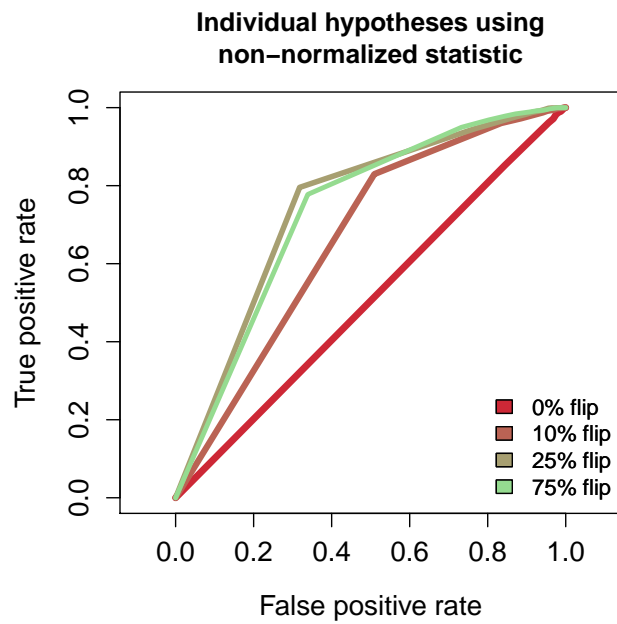


Figure 12: The RoC curves for Stepdown method for the non-normalized statistic. The format is the same as in Figure 6. Comparing this figure to Figure 6, we see that the non-normalized method is less powerful.